Supplementary Information

Modulating paired Ir-O-Ir via electronic perturbations of correlated Ir single atoms to overcome catalytic selectivity

Shi-Hua Chen,[a,b,‡] Yuan-Fan Yang,[a,c,‡] Zong-Yin Song,[a,c] Xiang-Yu Xiao,[a,c] Cong-Cong Huang [a,c], Xin Cai [a,c], Pei-Hua Li,[a] Meng Yang,[a] Aicheng Chen,[d] Wen-Qing Liu,[e,*], Xing-Jiu Huang [a,b,c,*]

[a] Key Laboratory of Environmental Optics and Technology, And Environmental Materials and Pollution Control Laboratory, Institute of Solid State Physics, HFIPS, Chinese Academy of Sciences, Hefei 230031, China

[b] State Key Laboratory of Transducer Technology, Shanghai Institute of Microsystem And Information Technology, Chinese Academy of Sciences, Shanghai 200050, China

[c] Department of Materials Science and Engineering, University of Science and Technology of China, Hefei 230026, China

[d] Department of Chemistry, University of Guelph, Guelph, ON N1G 2W1, Canada

[e] Anhui Institute of Optics and Fine Mechanics, HFIPS, Chinese Academy of Sciences, Hefei 230031, P. R. China

* Corresponding authors

E-mail : wqliu@aiofm.ac.cn; xingjiuhuang@iim.ac.cn.

[‡] S. H. Chen and Y. F. Yang contributed equally to this work.

Contents

3. Tables

1 Experimental Section

1.1 Chemical Reagents

The chemical reagents as follow were commercial with analytical grade and directly used in the experiments without any pretreatment. Cobalt nitrate hexahydrate ($Co(NO_3)_2 \cdot 6H_2O$), Hydrogen hexachloroiridate(IV) hexahydrate($H_2IrCl_6 \cdot 6H_2O$), Hexadecyl trimethyl ammonium Bromide(CTAB, $C_{19}H_{42}BrN$), and Sodium borohydride(SB, $NaBH_4$) were purchased from the Shanghai Reagent Company (P. R. China).

1.2 Material synthesis

Synthesis of Co_3O_4. Firstly, 4.0 mmol $Co(NO_3)_2 \cdot 6H_2O$ and 5.0 mmol CTAB were dissolved into 100 mL of water in turn. Then, 6.0 mmol SB was quickly added under stirring. After reacting for another 4 h. The resulting products were collected and washed with distilled water and acetone, and dried at 60 °C overnight. Finally, Co_3O_4 nanosheets were obtained by calcined the precursor at 450 °C for 4 h under air, and the heating rate was 5°C min^{-1}.

Synthesis of IrO_2/Co_3O_4. Firstly, 4.0 mmol $Co(NO_3)_2 \cdot 6H_2O$ and 5.0 mmol CTAB were dissolved into 100 mL of water in turn. Then, 8 mL $H_2IrCl_6 \cdot 6H_2O$(40 mg/ mL) was added into the above purple solution to get a blue-green solution under continuous stirring. Then, 8 mmol SB was quickly added under stirring. After reacting for 4 h, the resulting products were collected and washed with distilled water and acetone, and

dried at 60 °C overnight. Finally, IrO_2/Co_3O_4 nanosheets were obtained by calcined the precursor at 450 °C for 4 h under air, and the heating rate was 5°C min^{-1}.

1.3 Material characterization

Field-emission scanning electron microscopy (FESEM, Quanta 200 FEG, FEI Company, USA), was utilized for the morphology characterization of the prepared nanomaterials. Transmission electron microscopy (TEM), high-resolution TEM(HR-TEM) and energy-dispersive spectrometer (EDS) and selected area electron diffraction (SAED) were carried out with a JEM-2010 transmission electron microscope operating at 200 kV (quantitative method, Cliff Lorimer thin ratio section). The high-angle annular dark-field scanning transmission electron microscopy with a spherical aberration (HAADF-STEM, Ac-STEM, JEOL ARM-200F). X-ray diffractometer patterns of the nanomaterials were performed with a Philips X'PertPro X-ray diffractometer (Cu Kα radiation λ=1.5418 Å). X-ray photoelectron spectroscopy (XPS) measurements were achieved using a VGESCALAB MKII spectrometer with an Mg Kα X-ray source (1253.6 eV, 120 W). Brunauer-Emmett-Teller (BET) measurements were implemented with the specific surface area and porosity analyzer (ASAP2460). Raman spectra were obtained by a Lab RAM HR800 confocal microscope Raman system (Horiba Jobin Yvon, Inc., USA). The content of Ir was determined by ICP-AES (Jarrell-Ash model, ICAP 9000, Wavelength: 1890 nm).

All electrochemical measurements were performed with a CHI 660D computer-controlled potentiostat (ChenHua Instruments Co., Shanghai, China), including a standard three-electrode system, with a platinum wire, Ag/AgCl (3 mol L^{-1} KCl) electrode and a bare or modified glassy carbon electrode (GCE) as the counter electrode, reference electrode and the working electrode, respectively.

1.4 Fabrication of modified electrodes

Firstly, 1.0 mg/mL aqueous solutions of the prepared nanomaterials were respectively configured. Then, 5 μL above solutions were separately taken and dropped onto the surface of the pre-treated glass carbon electrode (GCE), which has been polished by 0.05 μM Al_2O_3 powder and washed by successively ultrasounding for 20 s with diluted HNO_3, ethanol and deionized water. After fully drying, Ir SAs/Co_3O_4/GCE, Co_3O_4/GCE and IrO_2/Co_3O_4/GCE were obtained for the electrochemical measurements.

1.5 Active area of modified electrodes

The electrochemical active electrode surface area of the modified electrodes was characterized by CV in 5 mM $Fe(CN)_6^{3-/4-}$ containing 0.1 M KCl at scan rates range from 0.01 V to 0.20 V, according to the Randles-Sevcik equation at 298 K, $i_p = (2.69 \times 10^5)\, n^{3/2} A c_0 D_0^{1/2} v^{1/2}$, where, A is the area in cm^2, D_0 is the diffusion coefficient in cm^2

s^{-1}, c_0 is the concentration in mol cm^{-3}, v is the scan ratee in V s^{-1} and i_p is the peak current in amperes. Besides, D_0 for $K_4Fe(CN)_6$ is $6.61x10^{-6}$ cm^2 s^{-1}.

1.6 Electrochemical measurements and optimization

Cyclic voltammetry (CV) and Electrochemical impedance spectroscopy (EIS) were tested in 0.1 M KCl including 5 mM $K_3Fe(CN)_6$. Besides, for EIS, the applied potential was set as the average value of the peak potential obtained by the CV test, with a scan rate of 0.1 V/s, frequency range from 1 to 100000 Hz, and amplitude of 0.005 V. All of the electrochemical detection was carried out using the square wave anodic stripping voltammetry (SWASV). The kinds and pH of the supporting electrolyte, deposition potential and run time were optimized, through changing one condition, comparing the SWASV signals toward 5 ppb As(III).

1.7 Determination of turnover frequencies

Turnover frequency (TOF) is the number of reactants consumed per unit of the active site per unit of time[1], so the TOF value for reduction of As(III) was calculated as the following equation：

$$TOF = \frac{N}{A \times t} \quad (1)$$

N is the number of As(III) participating in the electrocatalytic reduction process. A is the active area of the electrode interface (nm^2). *t* is the actual reaction time (s). In this study, N was obtained via equation (2)(3)(4)

$$N = \frac{Q}{3 \times e} \quad (2)$$

$$t = \frac{\Delta U}{v} \quad (3)$$

$$Q = It = I\frac{\Delta U}{v} = \frac{\int_{U1}^{U2} I(U)dU}{v} \quad (4)$$

where Q is the total coulomb of transferred electrons (C) during the reduction process, and $\int_{U1}^{U2} I(U)dU$ could be computed by the integral over the area of the LSV curves. ΔU (V) is the range of potential that the electrocatalytic reaction occurs, and ν is the scan rate (V/s). Thus, the determined N for Ir SAs/Co_3O_4/GCE was

$$N = \frac{3.3888 \times 10^{-6}\,C}{3 \times 1.60 \times 10^{-19}C \times 0.1\ V/s} \approx 7.06 \times 10^{13}$$

N for IrO_2/Co_3O_4/GCE was

$$N = \frac{1.7093 \times 10^{-7}\,C}{3 \times 1.60 \times 10^{-19}C \times 0.1\ V/s} \approx 3.56 \times 10^{12}$$

N for Co_3O_4/GCE was

$$N = \frac{5.2804 \times 10^{-8}\,C}{3 \times 1.60 \times 10^{-19}C \times 0.1\ V/s} \approx 1.10 \times 10^{12}$$

The actual reaction time t (s) was calculated using equation (3).

Thus, the determined t for Ir SAs/Co_3O_4/GCE was $t = \frac{0.30\ V}{0.1\ v/s} = 3.0\ s$

For IrO_2/Co_3O_4/GCE, $t = \frac{0.18\ V}{0.1\ v/s} = 1.8\ s$

For Co_3O_4/GCE, $t = \frac{0.12\ V}{0.1\ v/s} = 1.2\ s$

Therefore, for Ir SAs/Co_3O_4/GCE catalysts on As(III),

$$TOF_{Ir\ SAs/Co_3O_4/GCE} = \frac{N}{A \times t} = \frac{7.06 \times 10^{13}}{5.27 \times 10^{12}\ nm^2 \times 3.0\ s} \approx 4.47\ (nm^2\ s^{-1})$$

For IrO_2/Co_3O_4/GCE catalysts on As(III),

$$TOF_{IrO_2/Co_3O_4/GCE} = \frac{N}{A \times t} = \frac{3.56 \times 10^{12}}{4.37 \times 10^{12} nm^2 \times 1.8\ s} \approx 0.45\ (nm^2\ s^{-1})$$

For Co_3O_4/GCE catalysts on As(III),

$$TOF_{Co_3O_4/GCE} = \frac{N}{A \times t} = \frac{1.10 \times 10^{12}}{3.38 \times 10^{12}\ nm^2 \times 1.2\ s} \approx 0.27\ (nm^2\ s^{-1})$$

1.8 Adsorption experiments

Adsorption experiments were carried out in a 0.1 M HAc-NaAc of pH=5. The concentration of samples is 1 mg/mL and the concentration of As(III) is 10 ppm, the mixture was shaking at 15 °C for 1 day at a speed of 200 rpm. After washed by 0.1 M HAc-NaAc (pH=5) for 1-2 times, the deposit was collected and freeze-dried for further XPS and XAFS analysis.

1.9 XAFS analysis

The X-ray absorption fine structure (XAFS) spectra of Co K-edge were acquired in transmission mode, and Lytle-fluorescence mode for As K-edge and Ir L_3-edge at the BL14W and BL11B beamline of Shanghai Synchrotron Radiation Facility (SSRF). Athena and Artemis included in the IFEFFIT software packages were used to analyze data. In detail, X-ray absorption near edge structure spectra(XANES) of the Co K-edge, As K-edge and Ir L_3-edge were normalized to analyze the valence of corresponding elements. Besides, k^3-weighted $\chi(k)$ data in the k space were Fourier transformed(FT)

to radial structure functions to separate the extended X-ray absorption fine structure (EXAFS).

1.10 DFT calculations

All DFT calculations were performed using the Vienna Ab initio Simulation Package (VASP)[2]. The projector augmented wave (PAW)[3] pseudopotential with the PBE[4] generalized gradient approximation (GGA) exchange correlation function was utilized in the computations. All energetics of metal oxides were calculated using the DFT with the Hubbard-U framework (DFT+U) to account for strongly localized d-electrons for Co (U_{eff} = 3.32 eV)[5]. The cutoff energy of the plane waves basis set was 500 eV and a Monkhorst-Pack mesh of 3×3×1 was used in K-sampling in the calculation of adsorption energy and 9×9×1 was used in the calculation of DOS and charge density difference. All structures were spin polarized and all atoms were fully relaxed with the energy convergence tolerance of 10^{-5} eV per atom, and the final force on each atom was < 0.05 eV $Å^{-1}$.

The adsorption energy of reaction intermediates, can be computed using the following Equation (1):

$$\Delta G_{ads} = E_{*\,ads} - E_{*+\,ads} + \Delta E_{ZPE} - T\Delta S \quad (1)$$

Where ads = (*H_3AsO_3, *H_2AsO_2, *HAsO and *As), and ($E_{*\,ads} - E_{*+\,ads}$) is the binding energy, ΔE_{ZPE} is the zero-point energy change, ΔS is the entropy change. In this work, the values of ΔE_{ZPE} and ΔS were obtained by vibration frequency calculation.

The Gibbs free energy of the reaction steps can be calculated by the following the Equations (2)-(5):

$$* + H_3AsO_3 = *H_3AsO_3 \quad (2)$$

$$*H_3AsO_3 + H^+ + e^- = *H_2AsO_2 + H_2O \quad (3)$$

$$*H_2AsO_2 + H^+ + e^- = *HAsO + H_2O \quad (4)$$

$$*HAsO + H^+ + e^- = *As + H_2O \quad (5)$$

Supplementary Figures

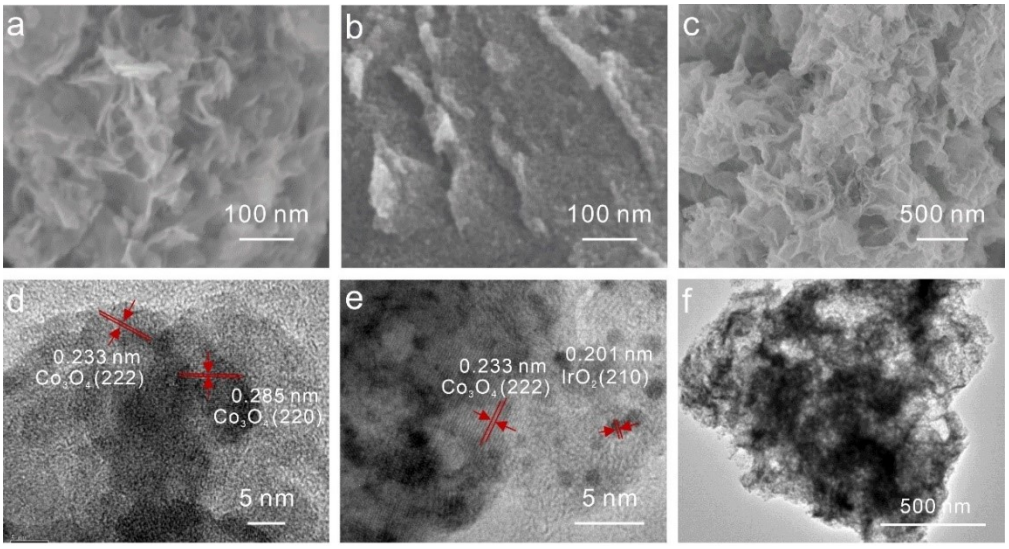

Fig. S1 Morphological Characterizations. SEM images of (a) Co_3O_4, (b) IrO_2/Co_3O_4, and (c) Ir SAs/Co_3O_4. TEM images of (d) Co_3O_4, (e) IrO_2/Co_3O_4, and (f) Ir SAs/Co_3O_4.

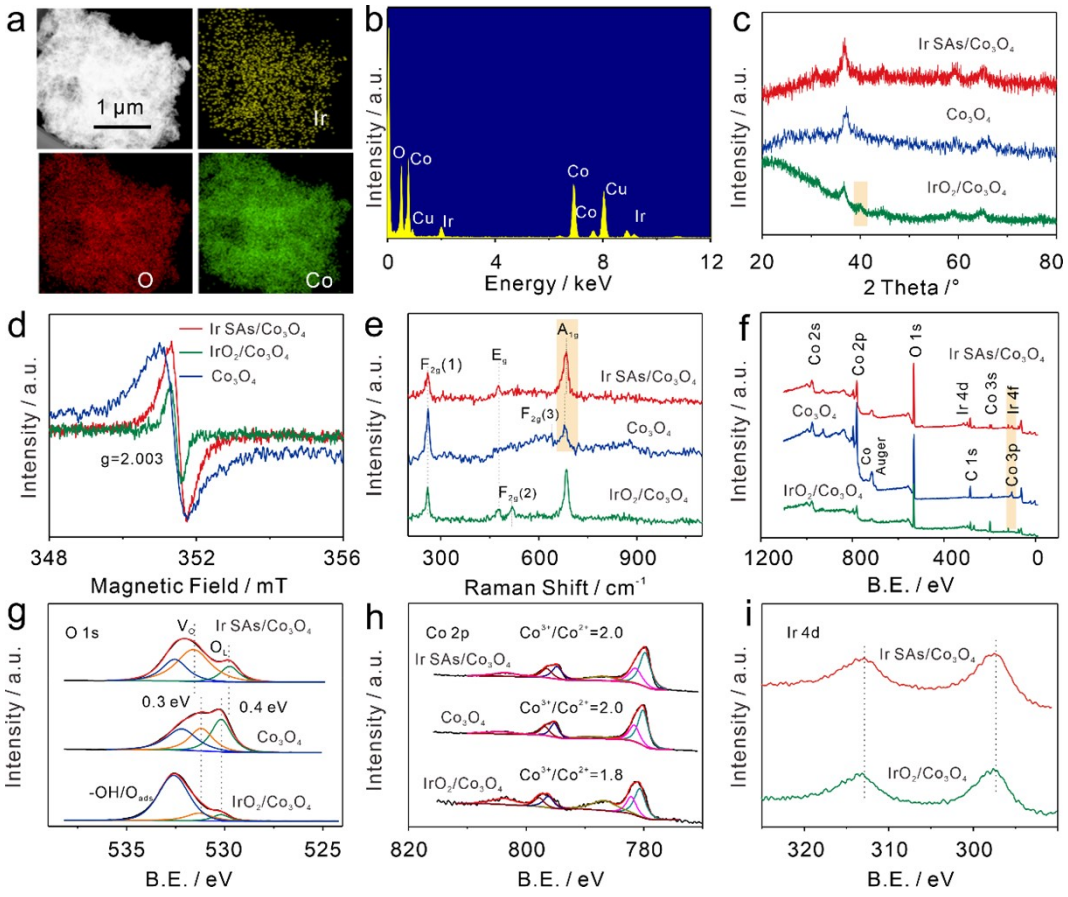

Fig. S2 Morphological and Structural Characterizations. (a) STEM image and elemental mapping of Ir, O, and Co in Ir SAs/Co_3O_4. (b) EDS patterns of Ir SAs/Co_3O_4.

(c) XRD patterns. (d) EPR spectra. (e) Raman spectra. (f) XPS survey of Ir SAs/Co_3O_4, Co_3O_4, and IrO_2/Co_3O_4. HR-XPS spectra in (g) O 1s, (h) Co 2p, and (i) Ir 4d.

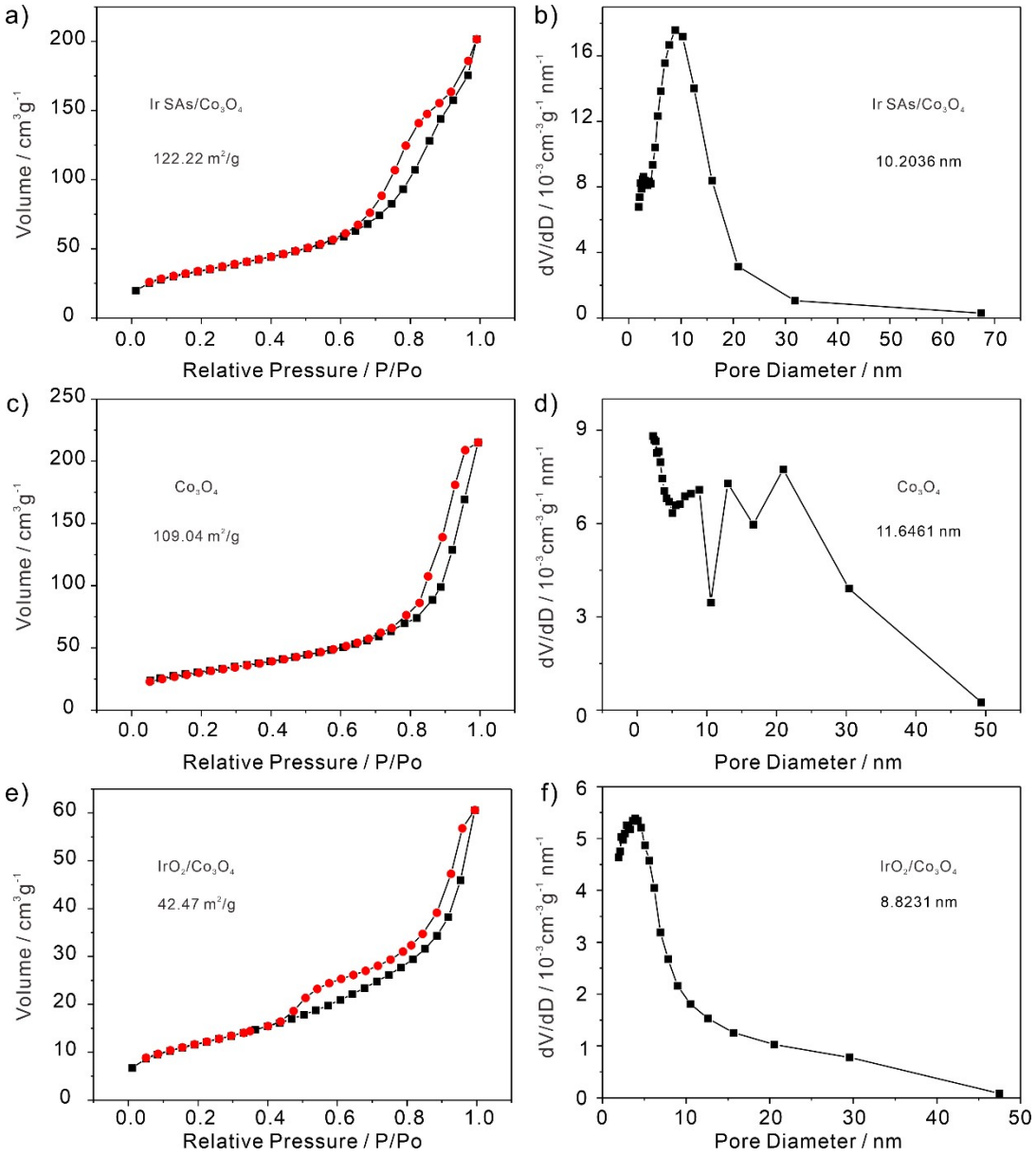

Fig. S3. BET and the aperture distribution of Ir SAs/Co_3O_4, Co_3O_4, and IrO_2/Co_3O_4.

BET measurements were used to characterize the surface areas and the porous structures of the prepared samples. The N_2 adsorption-desorption isotherms, and the suiting aperture distribution of Ir SAs/Co_3O_4, Co_3O_4, and IrO_2/Co_3O_4 are presented in Fig. S3. The surface areas of them were calculated to be 122.2, 109.0 and 42.5 m^2/g,

and most of the mesoporous structures were approximately10.2, 11.6 and 8.8 nm, respectively, corresponding to the results revealed by TEM images.

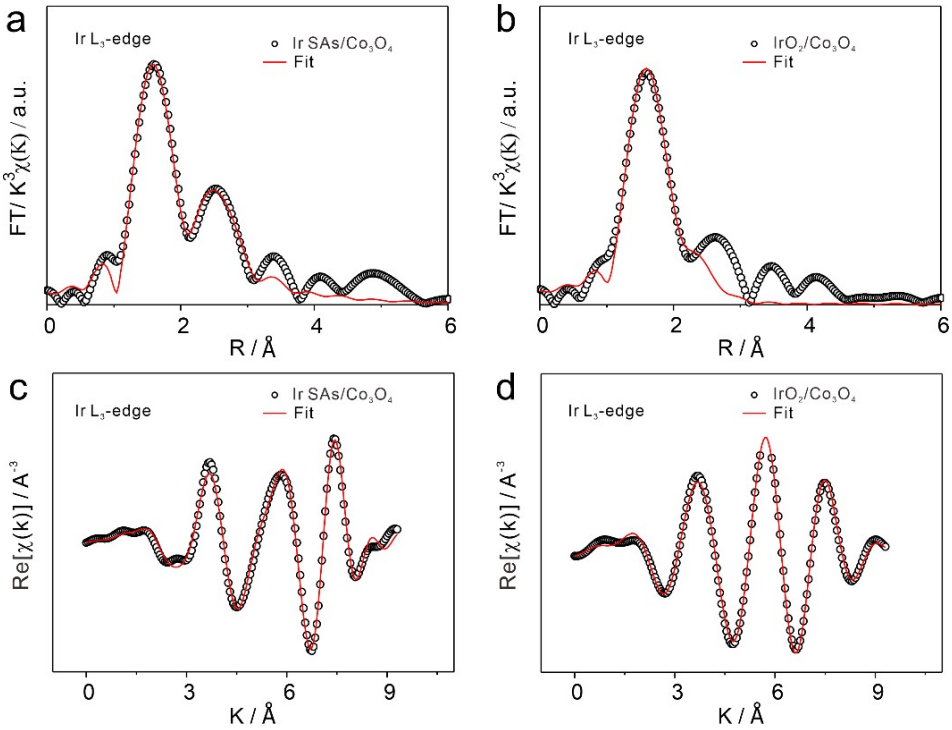

Fig. S4 XFAS analysis and fitting results of Ir L_3-edge. FT-EXAFS k^3-weighted χ(k) function spectra and fitting results (uncorrected for phase shift) for Ir L_3-edge of (a) Ir SAs/Co_3O_4, and (b) IrO_2/Co_3O_4. k^3-weighted k-space spectra for Ir L_3-edge and fitting spectra of (c) Ir SAs/Co_3O_4, and (d) IrO_2/Co_3O_4.

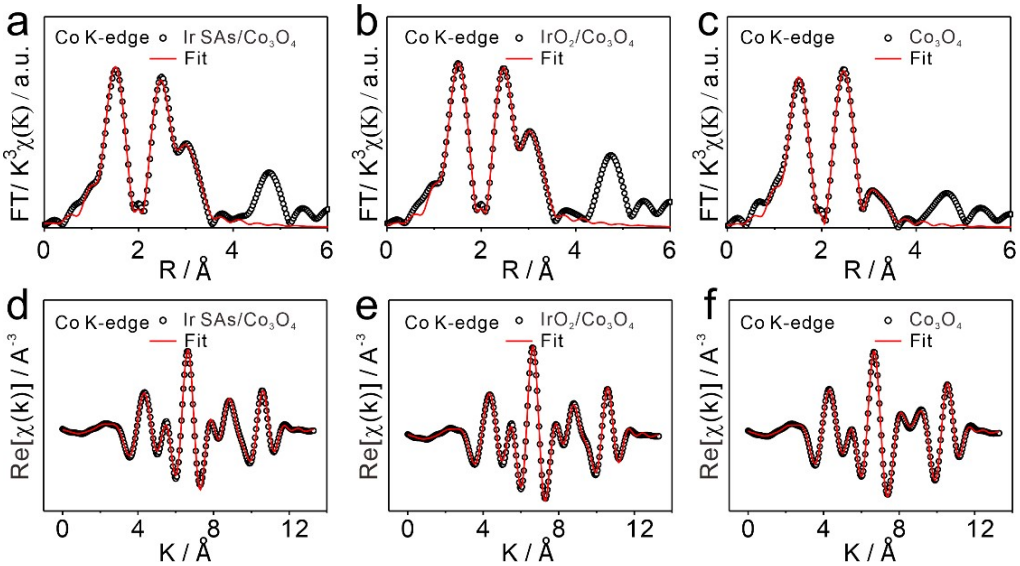

Fig. S5 XFAS analysis and fitting results of Co K-edge. FT-EXAFS k^3-weighted χ(k)

function spectra and fitting results (uncorrected for phase shift) for Co K-edge of (a) Ir SAs/Co_3O_4, (b) IrO_2/Co_3O_4, and (c) Co_3O_4. k^3-weighted k-space spectra for Co K-edge and fitting spectra of (d) Ir SAs/Co_3O_4, (e) IrO_2/Co_3O_4, and (f) Co_3O_4.

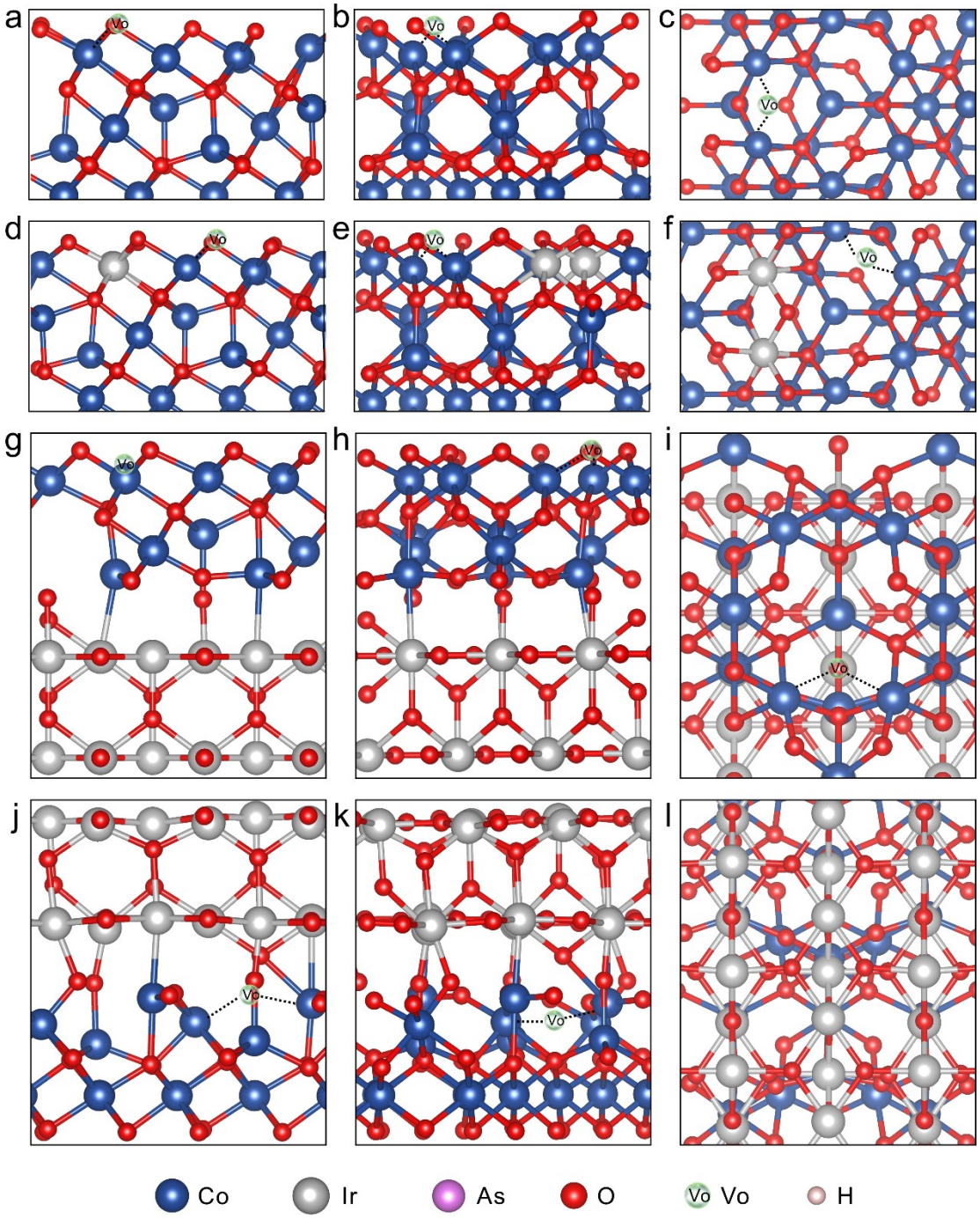

Fig. S6 The front, side and top view of the optimized configurations. (a-c) Co_3O_4. (d-f) Ir SAs/Co_3O_4. (g-i) IrO_2/Co_3O_4(Co) and (j-l) IrO_2/Co_3O_4-(Ir).

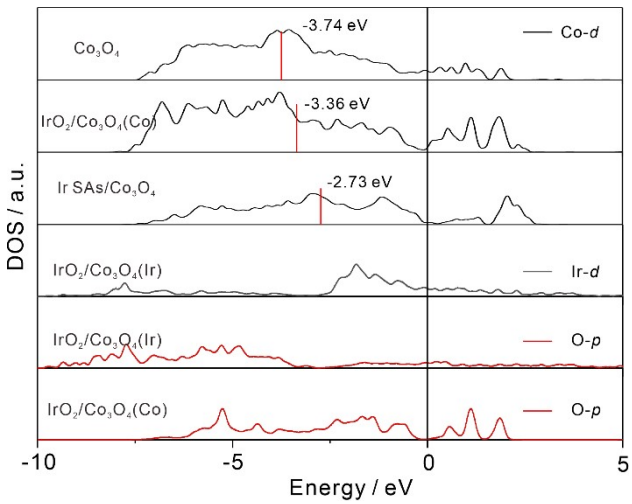

Fig. S7 DOS of Co_3O_4, IrO_2/Co_3O_4(Co), IrO_2/Co_3O_4(Ir) and Ir SAs/Co_3O_4.

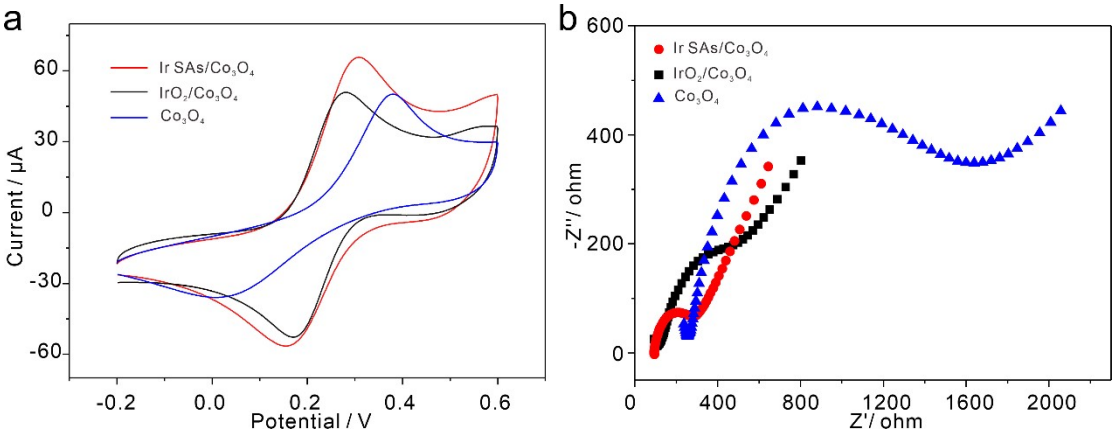

Fig. S8 Electrochemical characterization of GCE modified by Ir SAs/Co_3O_4, IrO_2/Co_3O_4 and Co_3O_4. (a) CV. (b) EIS.

CV curves in **Fig. S8a** shows that the current of Ir SAs/Co_3O_4/GCE higher than that of IrO_2/Co_3O_4 /GCE, and Co_3O_4/GCE. The corresponding EIS data in **Fig. S8b** further revealed that the resistance of Ir SAs/Co_3O_4/GCE was smaller than that of IrO_2/Co_3O_4 /GCE, and Co_3O_4/GCE, indicating that Ir SAs/Co_3O_4/GCE has high conductivity and rapid redox reaction.

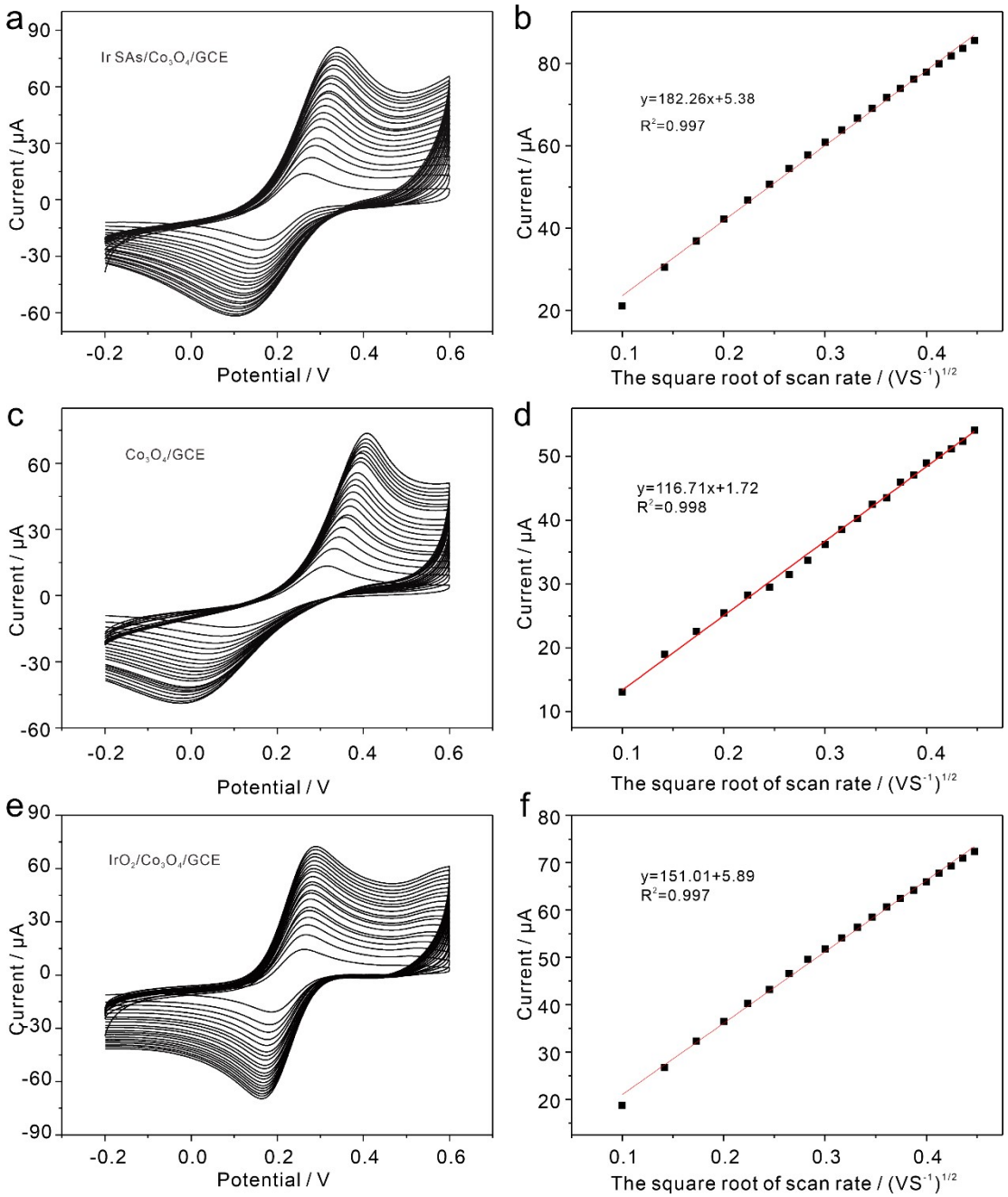

Fig. S9 Tests of electrochemical active electrode surface area. Scan rate study (from 0.01 to 0.2 V s^{-1}) at (a) Ir SAs/Co_3O_4/GCE, (c)Co_3O_4/GCE, and (e) IrO_2/Co_3O_4/GCE in the solution of 5 mM $K_3[Fe(CN)_6]$, respectively. (b), (d) and (f) the corresponding plot of current versus the square root of the scan rate with a linear trend line.

The electrochemical active electrode surface area of Ir SAs/Co_3O_4/GCE, Co_3O_4/GCE and IrO_2/Co_3O_4/GCE was calculated to be 0.0527, 0.0338, and 0.0437 cm^2.

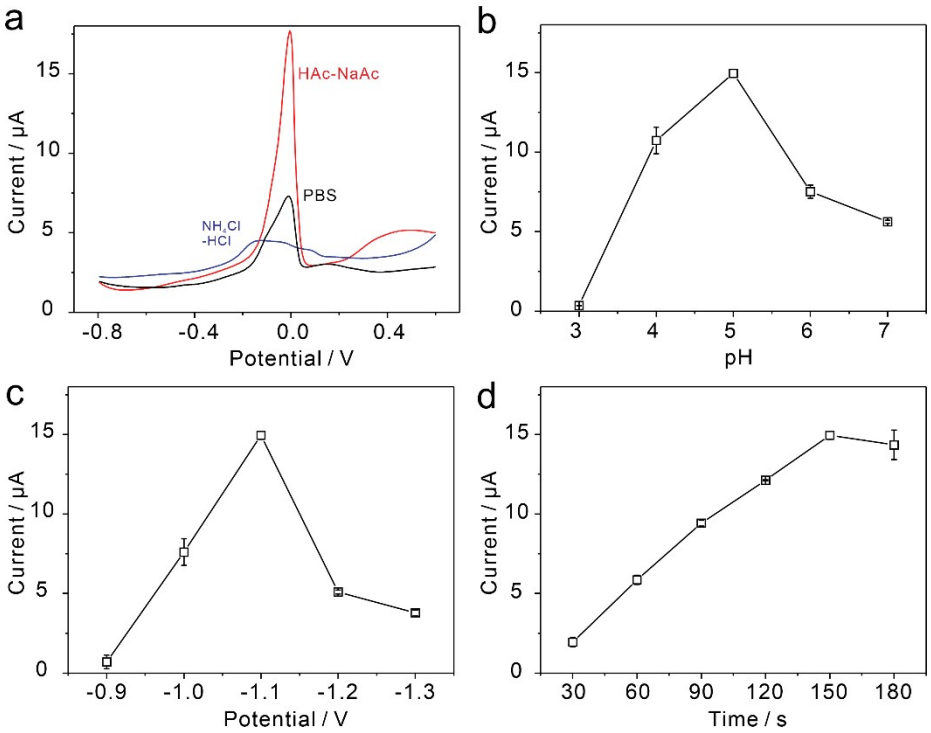

Fig. S10 SWASV conditions optimization with 5 ppb As(III) on Ir SAs/Co_3O_4/GCE. Individually change: (a) buffer solution. (b) pH value of HAc-NaAc. (c), (d) deposition potential and time.

In general, 0.1 M HAc-NaAc solution (pH=5) was employed as the electrolyte, and the deposition potential and time were set as -1.1 V and 150 s in the detection process.

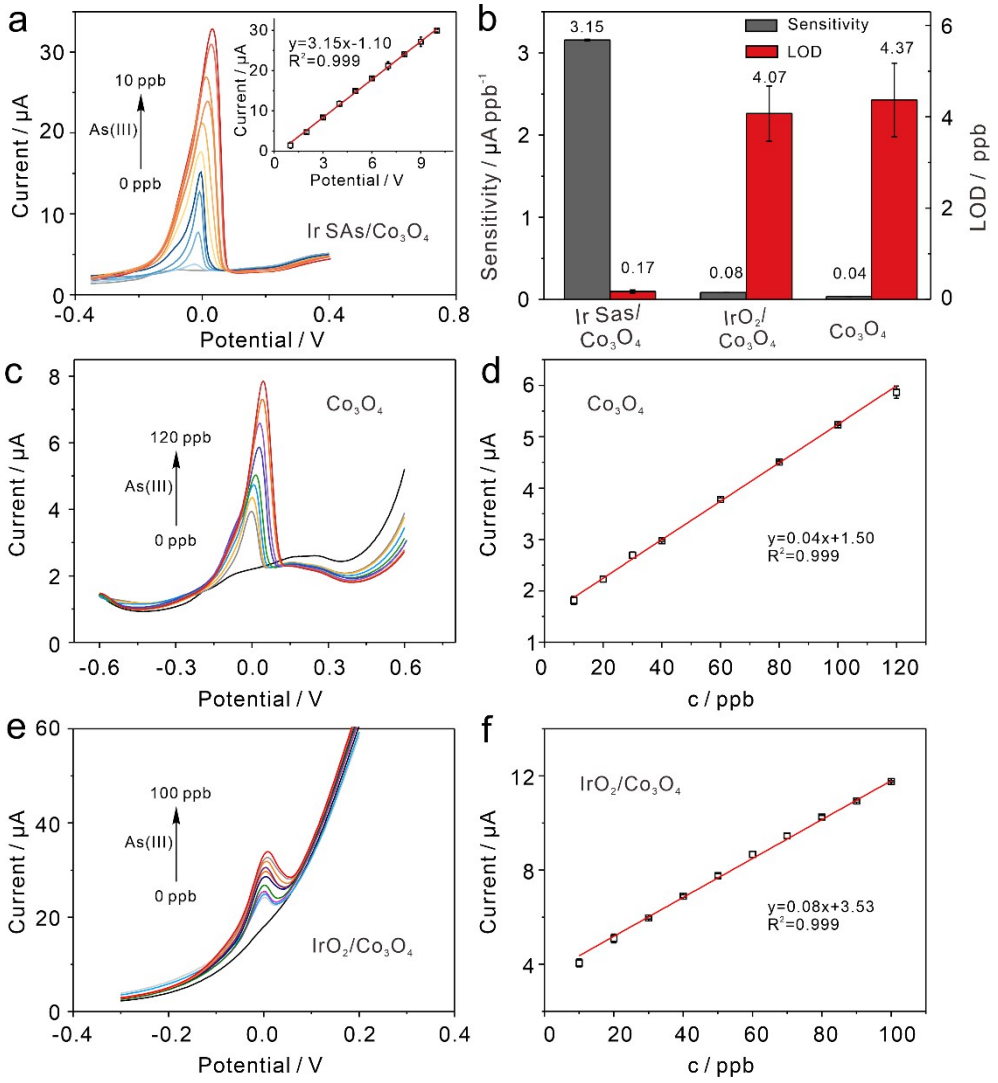

Fig. S11 SWASV responses toward As(III) of different catalysts. (a) SWASV responses and linear equations (inset) of Ir SAs/Co_3O_4/GCE. (b) Sensitivity and LOD toward As(III) of different modified electrodes. (c), (d) SWASV responses and linear equations of Co_3O_4/GCE; (e), (f) SWASV responses and linear equations of IrO_2/Co_3O_4/GCE.

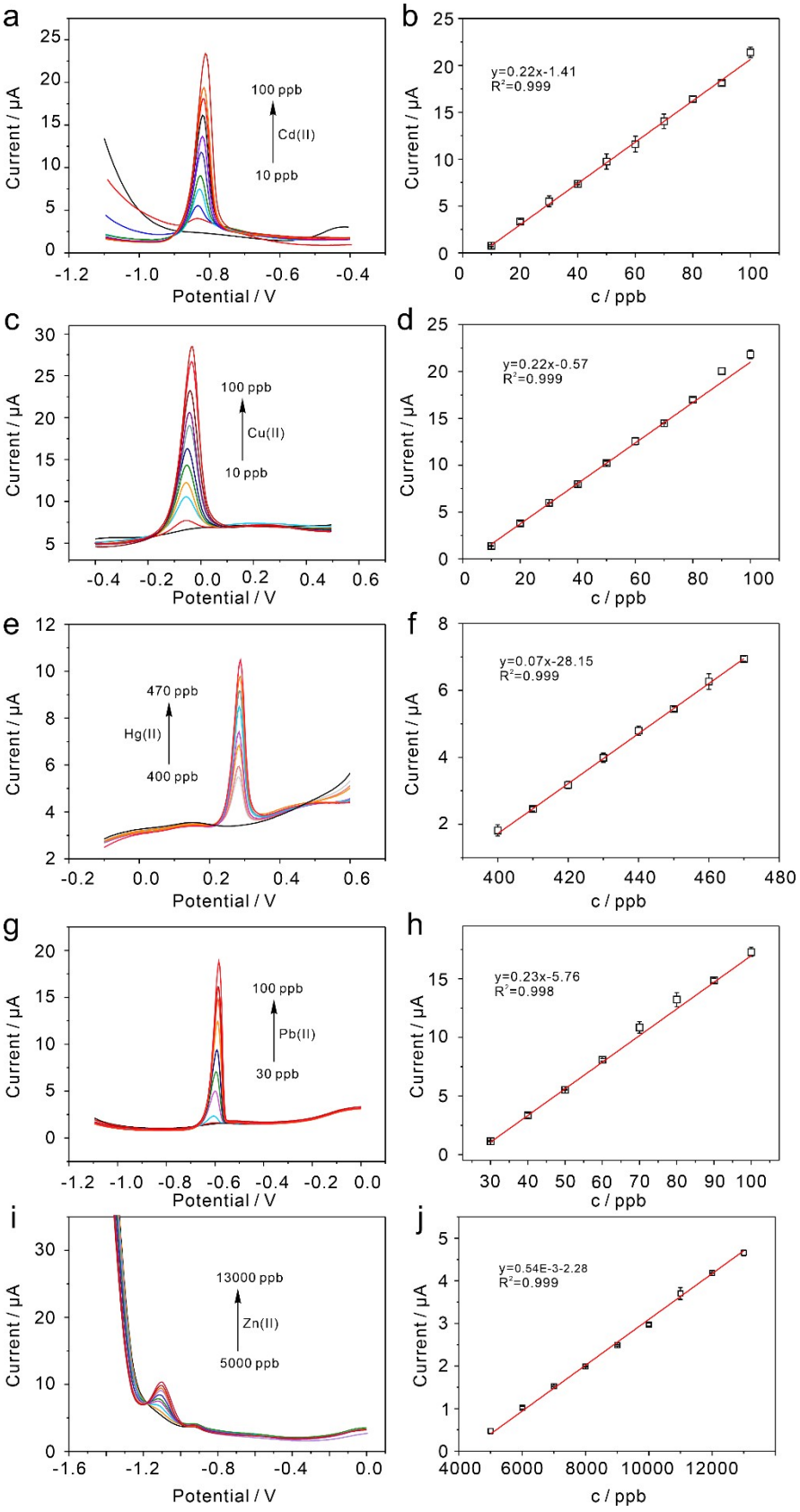

Fig. S12 SWASV responses of Ir SAs/Co_3O_4/GCE and corrsponding linear equations toward different HMIs. (a), (b) Cd(II). (c), (d) Cu(II). (e), (f) Hg(II). (g), (h) Pb(II). (i), (j) Zn(II).

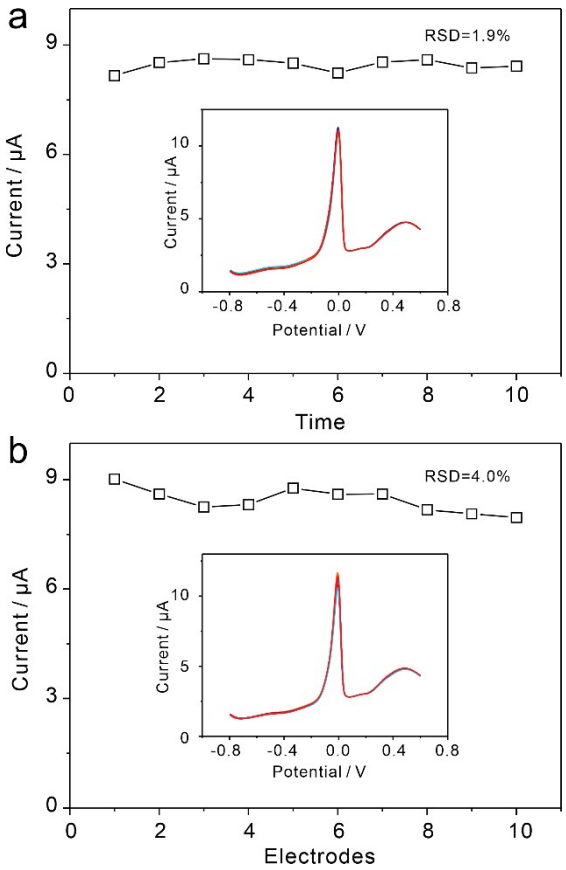

Fig. S13 Stability and reproducibility tests. (a) stability tests. (b) reproducibility tests. Insets of (a) and (b) show the detailed SWASV signals toward As(III) of 4 ppb.

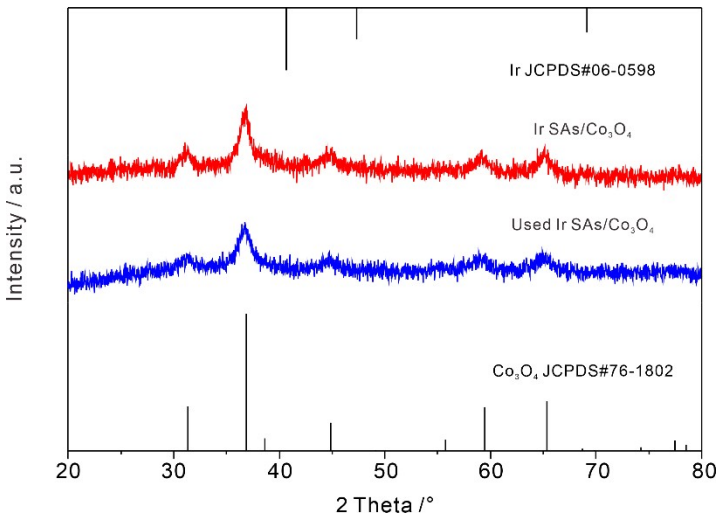

Fig. S14 XRD patterns of Ir SAs/Co_3O_4 before and after electrochemical tests and the characteristic peaks of Ir and Co_3O_4.

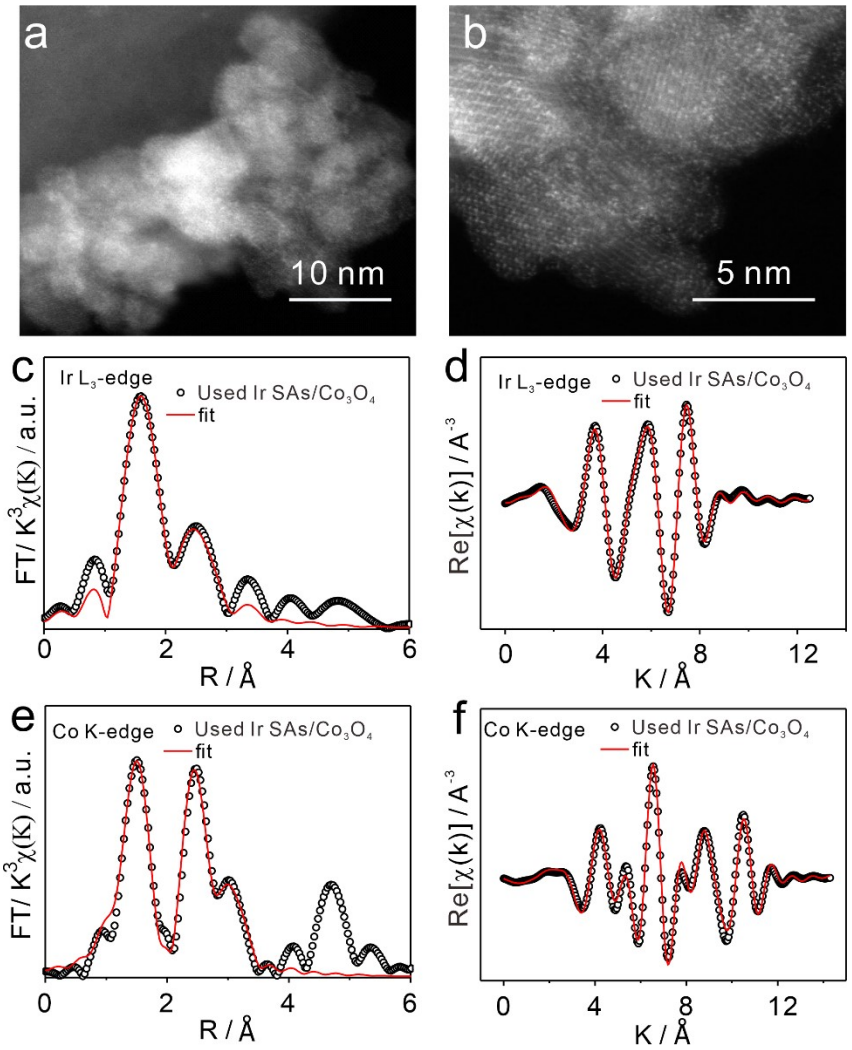

Fig. S15 Durability tests of Ir SAs/Co_3O_4 after electrochemical tests of 20 times. (a), (b) HADDF-STEM image collected on randomly chosen domains. k^3-weighted and fitting spectra (uncorrected for phase shift) for Ir L_3-edge of used Ir SAs/Co_3O_4 in (c) R-space (d) K-space. k^3-weighted and fitting spectra (uncorrected for phase shift) for Co K-edge of used Ir SAs/Co_3O_4 in (e) R-space and (f) K-space.

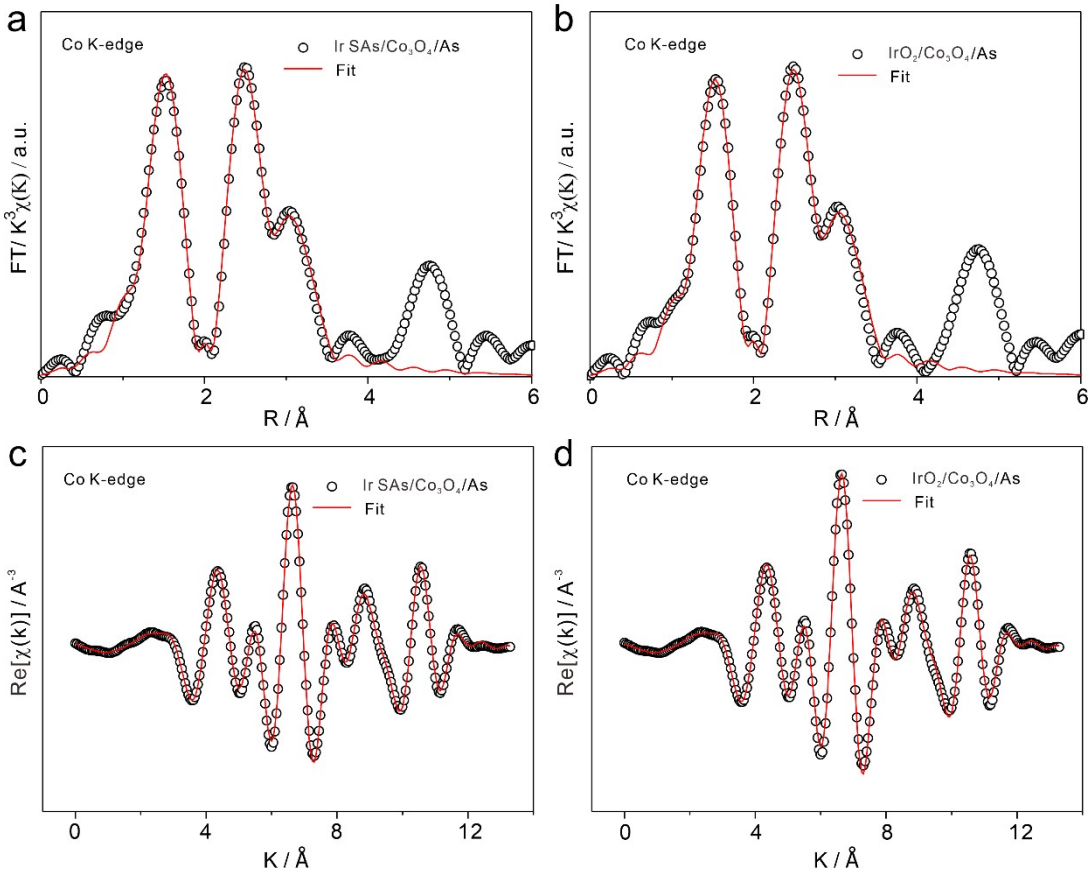

Fig. S16 XFAS analysis and fitting results of Co K-edge after interacting with As(III). FT-EXAFS k^3-weighted χ(k) function spectra and fitting results (uncorrected for phase shift) for Co K-edge of **(a)** Ir SAs/Co_3O_4-As, and **(b)** IrO_2/Co_3O_4-As. k^3-weighted k-space spectra for Co K-edge and fitting spectra of **(c)** Ir SAs/Co_3O_4-As, and **(d)** IrO_2/Co_3O_4.

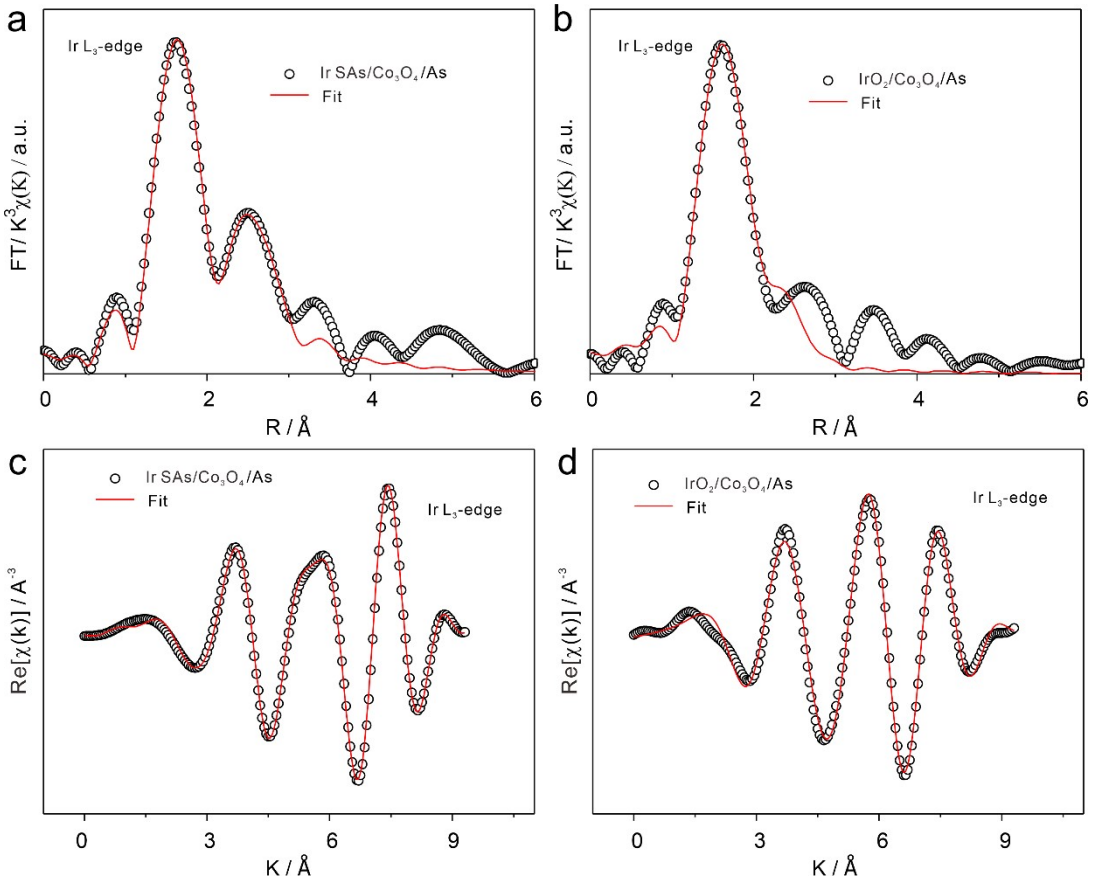

Fig. S17 XFAS analysis and fitting results of Co K-edge after interacting with As(III). FT-EXAFS k^3-weighted χ(k) function spectra and fitting results (uncorrected for phase shift) for Ir L_3-edge of (a) Ir SAs/Co_3O_4-As, and (b) IrO_2/Co_3O_4-As. k^3-weighted k-space spectra for Ir L_3-edge and fitting spectra of (c) Ir SAs/Co_3O_4-As, and (d) IrO_2/Co_3O_4-As.

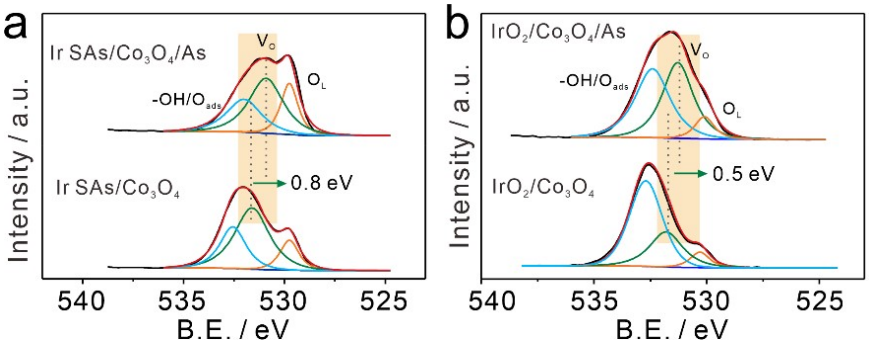

Fig. S18 HR-XPS spectra in O 1s before and after interacting with As(III). (a) Ir SAs/Co_3O_4. (b) IrO_2/Co_3O_4/As.

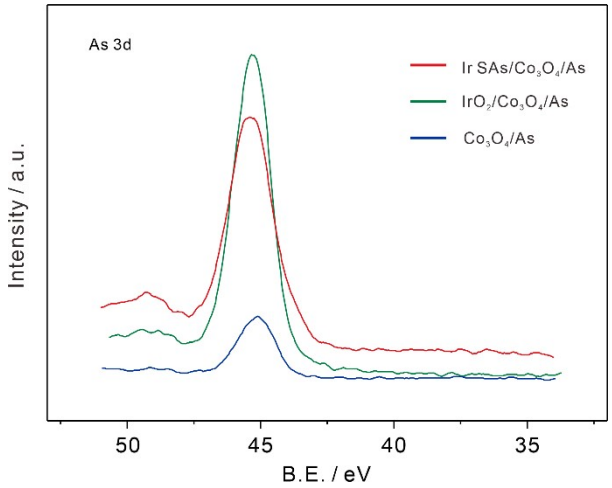

Fig. S19 HR-XPS spectra in As 3d in Ir SAs/Co_3O_4. (b) IrO_2/Co_3O_4/As.

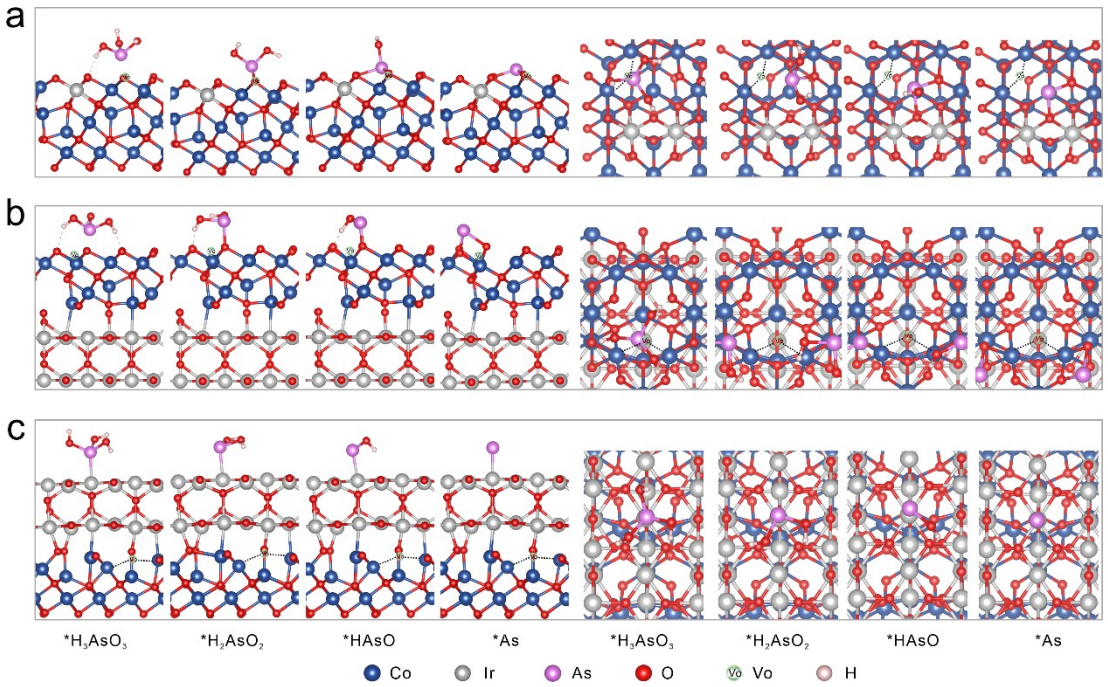

Fig. S20 Front and top view of the adsorption and stepwise reduction configurations of H_3AsO_3. (a) Ir SAs/Co_3O_4. (b) IrO_2/Co_3O_4(Co). (c) IrO_2/Co_3O_4(Ir).

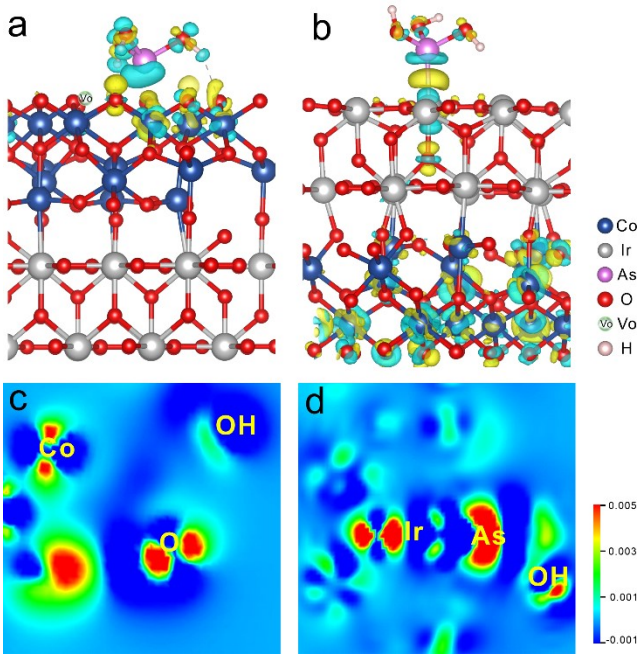

Fig. S21 Charge density difference image. (a) $IrO_2/Co_3O_4(Co)/As$. (b) $IrO_2/Co_3O_4(Ir)/As$. The isovalue is 0.005 eV/Å^3, and the green areas represent the depletion of electrons, while the yellow areas represent the accumulation of electrons. (c) Charge density difference images of $IrO_2/Co_3O_4(Co)/As$ on the slice through Co, O and O in H_3AsO_3. (d) Charge density difference images of $IrO_2/Co_3O_4(Ir)/As$ on the slice through Ir, O and As. The blue areas represent the depletion of electrons, while the red areas represent the accumulation of electrons.

Supplementary Tables

Table. S1 EXAFS spectra fitting results of Ir L_3-edge in Ir SAs/Co_3O_4 and IrO_2/Co_3O_4 analyzed by the Artemis module of IFEFFIT (S_0^2=0.86).

Sample	Path	CN	R(Å)	σ^2(10^{-3} Å)	ΔE_0(eV)	R-factor
Ir SAs/Co_3O_4	Ir-O	6.0±0.9	**2.00±0.01**	2.8	10.1±1.5	0.0205
	Ir-Ir	4.0±0.6	2.98±0.01	2.0		
	Ir-Co	3.3±1.4	3.00±0.01	3.0		
IrO_2/Co_3O_4	Ir-O	5.1±0.4	1.99±0.01	5.0	10.4±2.5	0.0068
	Ir-Co	1.0±0.3	2.57±0.01	3.0		
Ir SAs/Co_3O_4/As	Ir-O	6.0±0.3	**2.03±0.01**	2.0	11.3±0.5	0.0045
	Ir-Ir	4.0±0.7	2.97±0.01	2.0		
	Ir-Co	3.1±1.3	3.00±0.01	2.0		
IrO_2/Co_3O_4/As	Ir-O	4.8±0.5	2.00±0.01	5.0	11.4±2.7	0.0154
	Ir-Co	1.0±1.0	2.57±0.01	3.0		
Used Ir SAs/Co_3O_4	Ir-O	6.0±0.3	2.00±0.01	2.8	10.2±1.1	0.0056
	Ir-Ir	4.7±1.4	2.98±0.01	2.0		
	Ir-Co	2.8±0.4	3.00±0.01	3.0		

Notes: CN, coordination number; R, distance between absorber and backscatter atoms. σ^2, Debye-Waller factor; ΔE_0, the inner potential difference between the reference compound and the experimental sample. R-factor, the goodness of fit.

Table. S2 EXAFS spectra fitting results of Co K-edge in Co_3O_4, Ir SAs/Co_3O_4 and IrO_2/Co_3O_4 analyzed by the Artemis module of IFEFFIT (S_0^2=0.70).

Sample	Path	CN	R(Å)	σ^2(10^{-3} Å)	ΔE_0(eV)	R-factor
Co_3O_4	Co-O	4.8±0.3	1.92±0.01	4.4	2.5±0.5	0.0022
	Co-Co	4.9±0.5	2.85±0.01	5.9		
	Co-Co	1.8±0.2	3.38±0.01	7.0		
Ir SAs/Co_3O_4	Co-O	5.2±0.2	1.91±0.01	4.0	1.0±0.5	0.0077
	Co-Co	3.9±0.2	2.84±0.01	5.4		
	Co-Co	5.9±0.4	3.35±0.01	7.0		
IrO_2/Co_3O_4	Co-O	4.5±0.4	1.92±0.01	4.2	1.9±0.8	0.0042
	Co-Co	3.5±0.7	2.85±0.01	5.4		
	Co-Co	5.6±0.4	3.36±0.01	7.0		
Co_3O_4/As	Co-O	5.7±0.1	1.92±0.01	7.0	2.5±0.5	0.0022
	Co-Co	4.4±0.4	2.84±0.01	5.8		
	Co-Co	3.3±0.2	3.37±0.02	7.0		
Ir SAs/Co_3O_4/As	Co-O	5.5±0.5	1.92±0.01	4.6	3.3±0.8	0.0051
	Co-Co	4.8±0.9	2.86±0.01	6.1		
	Co-Co	6.0±0.5	3.38±0.03	7.0		
IrO_2/Co_3O_4/As	Co-O	5.5±0.3	1.93±0.02	4.0	3.4±1.3	0.0052
	Co-Co	5.1±1.0	2.86±0.01	6.0		
	Co-Co	6.7±0.6	3.37±0.03	7.0		
Used Ir SAs/Co_3O_4	Co-O	5.6±0.4	1.91±0.01	4.0	3.2±0.9	0.0191
	Co-Co	3.9±0.3	2.85±0.01	5.0		
	Co-Co	5.0±0.4	3.35±0.01	6.8		

Notes: CN, coordination number; R, distance between absorber and backscatter atoms. σ^2, Debye-Waller factor; ΔE_0, the inner potential difference between the reference compound and the experimental sample. R-factor, the goodness of fit.

Table. S3 Bader charge of Co_3O_4, IrO_2, Ir SAs/Co_3O_4, IrO_2/Co_3O_4(Co) and IrO_2/Co_3O_4(Ir).

	Ir	Co	Ir_{ads}	Co_{ads}
Co_3O_4	-	1.34	-	-
IrO_2	1.38	-	-	-
Ir SAs/Co_3O_4	1.75	1.35	1.80	1.37
IrO_2/Co_3O_4(Co)	-	1.30	-	1.41
IrO_2/Co_3O_4(Ir)	1.36	-	1.31	-

Table. S4 Comparison of electrochemical conditions and performance of other nanomaterial modified electrodes for As(III) detection.

Electrodes	Methods	Electrolyte	Diameter of Electrode mm	Detection Range ppb	Sensitivity μA ppb^{-1}	LOD ppb	Ref.
rGO/Fe_3O_4/GCE	SWASV	0.1 M PBS (pH 5.0)	3	0.1-20	0.281	0.12	6
CoO_x/GCE	CV	0.1 M PBS (pH 7.0)	2	15-300	0.00148	0.825	7
rGO/MnO_2NH/GCE	SWASV	0.1 M AcB (pH 5.0)	2	0.1-50	0.175	0.05	8
o-$CoSe_{2-x}$|P/GCE	SWASV	0.1 M AcB (pH 5.0)	3	1-10	1.11	0.15	9
AuNPs/α-MnO_2/GCE	SWASV	0.2 M CBS (pH 9.0)	3	1-10	0.828	0.019	10
$MnFe_2O_4$/Au/GCE	SWASV	0.1 M AcB (pH 5)	-	10-110	0.315	3.37	11
MnO_x/Au NPs-GCE	LSASV	0.1 CBS (pH 10.0)	-	0.5–80	2.749	0.05	12
ZrO_2/ Nafion /Au electrode	CV	PBS (pH 7.4)	2	5-60	0.550	5	13
AuNPs /CeO_2-ZrO_2/GCE	SWASV	0.1 M AcB (pH 8.0)	3	0.5-15	0.976	0.137	14
Au-RGO /GCE	LSASV	0.2M HCl (pH 0.7)	3	0.3-20	1.20	0.1	15
Co_3O_4 /GCE	SWASV	0.1 M AcB (pH 5.0)	3	10-120	0.04	4.37	This work
IrO_2	SWASV	0.1 M AcB	3	10-100	0.08	4.07	This

/Co_3O_4 /GCE		(pH 5.0)					work
Ir SAs /Co_3O_4 /GCE	SWASV	0.1 M AcB (pH 5.0)	3	1-10	3.15	0.17	This work

Notes: GCE: glass carbon electrode; rGO: reduced graphene oxide; DPASV: differential pulse anodic stripping voltammetry; PBS: phosphate buffer saline; CBS: Carbonate buffer solution; AcB: acetate buffer solution; CV: cyclic voltammetry; SWASV: square wave anodic stripping voltammetry; LSASV: Linear sweep anodic stripping voltammetry.

References

1. Z. Yuan, J. Li, M. Yang, Z. Fang, J. Jian, D. Yu, X. Chen and L. Dai, *J. Am. Chem. Soc.*, 2019, **141**, 4972-4979.
2. G. Kresse and J. Furthmüller, *Phys. Rev. B*, 1996, **54**, 11169-11186.
3. P. E. Blochl, *Phys Rev B Condens Matter*, 1994, **50**, 17953-17979.
4. J. P. Perdew, K. Burke and M. Ernzerhof, *Phys. Rev. Lett.*, 1996, **77**, 3865.
5. A. Jain, S. P. Ong, G. Hautier, W. Chen, W. D. Richards, S. Dacek, S. Cholia, D. Gunter, D. Skinner and G. Ceder, *APL materials*, 2013, **1**, 011002.
6. P. Devi, C. Sharma, P. Kumar, M. Kumar, B. K. S. Bansod, M. K. Nayak and M. L. Singla, *J. Hazard. Mater.*, 2017, **322**, 85-94.
7. A. Salimi, H. Mamkhezri, R. Hallaj and S. Soltanian, *Sens. Actuators B*, 2008, **129**, 246-254.
8. P. Devi, B. Bansod, M. Kaur, S. Bagchi and M. K. Nayak, *Sens. Actuators B*, 2016, **237**, 652-659.
9. S. H. Chen, Z. Y. Song, X. Y. Xiao, H. Q. Huang, Y. F. Yang, P. H. Li, M. Yang and X. J. Huang, *Anal. Chem.*, 2022, **94**, 3211-3218.
10. M. Yang, X. Chen, T. J. Jiang, Z. Guo, J. H. Liu and X. J. Huang, *Anal. Chem.*, 2016, **88**, 9720-9728.
11. S. Zhou, X. Han, H. Fan and Y. Liu, *Sensors*, 2016, **16**, 935.
12. S. Wu, Q. Zhao, L. Zhou and Z. Zhang, *Electroanalysis*, 2014, **26**, 1840-1849.
13. G. Bhanjana, N. Dilbaghi, S. Chaudhary, K. H. Kim and S. Kumar, *Analyst*, 2016, **141**, 4211-4218.
14. M. Yang, P.-H. Li, W.-H. Xu, Y. Wei, L.-N. Li, Y.-Y. Huang, Y.-F. Sun, X. Chen, J.-H. Liu and X.-J. Huang, *Sens. Actuators B*, 2018, **255**, 226-234.
15. W.-W. Li, F.-Y. Kong, J.-Y. Wang, Z.-D. Chen, H.-L. Fang and W. Wang, *Electrochim. Acta*, 2015, **157**, 183-190.